Elevated Temperature Compressive Properties of Zr-Modified NiAl

J. DANIEL WHITTENBERGER and R.D. NOEBE

Small Zr additions are known to substantially affect the deformation behavior and strength of polycrystalline NiAl, yet little information is currently available regarding the high-temperature properties of such alloys. Utilizing prealloyed powder technology, a series of four NiAl alloys have been produced containing from 0.05 to 0.7 at. pct Zr. The creep behavior of these alloys was characterized in compression between 1000 and 1400 K at strain rates ranging from ~0.1 to 10^{-9} s^{-1}. All the Zr-modified alloys were significantly stronger than binary NiAl under lower temperature and faster strain-rate conditions; however, the single-phase materials (Zr ≤ 0.1 at. pct) and binary NiAl had similar strengths at high temperatures and slow strain rates. The two-phase NiAl-Ni_2AlZr alloys containing 0.3 and 0.7 at. pct Zr had nearly identical strengths. While the two-phase alloys were stronger than the single-phase materials at all test conditions, the degree of microstructural damage in the two-phase alloys due to internal oxidation during testing appeared to increase with Zr level. Balancing the poor oxidation behavior with the consistent strength advantage of the two-phase alloys, it is concluded that optimum elevated-temperature properties could be obtained in Heusler-strengthened NiAl containing between 0.1 and 0.3 at. pct Zr.

I. INTRODUCTION

ALTHOUGH the B2-ordered intermetallic NiAl has a number of promising properties that make it an attractive replacement material for superalloys (*i.e.*, high melting point, good thermal conductivity, moderate density, and excellent oxidation resistance), it has poor elevated-temperature strength and is seriously lacking in low-temperature tensile ductility and toughness.[1–5] Simple third-element additions have been and are currently being investigated as a means to improve both of these deficiencies. For example, small (<0.3 at. pct) amounts of Fe, Ga, or Mo may improve the low-temperature tensile ductility of NiAl single crystals,[1] while 0.3 to 1 at. pct Hf or Ta containing NiAl single crystals have high-temperature creep properties approaching those of first-generation single-crystal Ni-based superalloys.[1,5–7]

Unfortunately, while polycrystalline, nominally equiatomic NiAl routinely can be deformed from 0.5 to 3 pct in tension at room temperature,[8] third-element additions have not produced any significant improvement in ductility. In fact, most alloying additions to polycrystalline NiAl (with the possible exceptions of W,[9] Be,[10] and N[11]) tend to decrease the room-temperature ductility and increase the brittle-to-ductile transition temperature (BDTT).[4,8] Elevated-temperature strength of polycrystalline NiAl, on the other hand, can be significantly affected by third-element additions. Polvani *et al.*[12] demonstrated in 1976 that replacement of about 10 at. pct Al with Ti will yield polycrystalline NiAl-Ni_2AlTi alloys with creep properties approaching those of Ni-based superalloys. Much smaller alloying additions, a few percent or less, of Re,[9] or Hf, Nb, and Ta[13] also have been reported to significantly increase the elevated-temperature strength of polycrystalline NiAl under fast strain-rate conditions. However, under high-temperature and slow strain-rate conditions, the effectiveness of third-element additions, at least for Hf[14] and Nb,[15] is dramatically decreased.

In other work by Raj and co-workers,[16,17] even smaller additions of Zr, on the order of 0.05 at. pct, were also shown to be extremely effective in strengthening NiAl, at least at strain rates of 10^{-4} s^{-1}. Coupled with the extremely potent strengthening effect of Zr[16,17] is the substantial influence of this element on the overall mechanical behavior of NiAl. For example, 0.05 at. pct Zr increases the brittle-to-ductile transition temperature of NiAl from 550 to nearly 850 K,[16,17] while an alloying addition of 0.1 at. pct Zr raises the BDTT to 1050 K.[18] The increase in brittle-to-ductile transition temperature has been attributed to the segregation of Zr to the grain boundaries in NiAl[19] and the subsequent inhibition of grain boundary deformation mechanisms.[17,20] Small (0.1 at. pct) additions of Zr also dramatically alter the low cycle-fatigue behavior of NiAl at 1000 K.[21] By reducing creep damage, low levels of Zr significantly increase the response stresses and fatigue life of NiAl at low strain ranges. However, fatigue life at higher strain ranges is reduced compared to binary NiAl due to the lack of tensile ductility in NiAl-0.1Zr. Finally, small amounts of Zr vastly improve the cyclic oxidation behavior of NiAl[22] to the point where all oxidation-resistant nickel aluminide coatings or alloys contain Zr or some other reactive alloying addition.

In spite of all the research on NiAl alloyed with small amounts of Zr, no further efforts to exploit its strengthening effects have been undertaken. Regardless of the BDTT liability produced by Zr, it still is important to define the limits of this element in its ability to strengthen NiAl at elevated temperatures. If small Zr additions are able to provide effective creep resistance in polycrystalline NiAl, then such alloys should be studied with the intention of transferring the strengthening mechanism(s) to more ductile NiAl-based matrices or, alternatively, improving the low-temperature properties of the strong alloys.

J. DANIEL WHITTENBERGER and R.D. NOEBE, Materials Research Engineers, are with NASA Lewis Research Center, Cleveland, OH 44135.
Manuscript submitted June 30, 1995.

Table I. Chemistry, Characterization, and Processing Conditions for NiAl Alloys Containing Various Levels of Zr

Material ID (Heat Number)	Composition (At. Pct)					Lattice Parameter (nm)		Consolidation Parameters	Grain Size (μm)†
	Al	C	N	O	Zr	NiAl*	Ni_2AlZr**		
NiAl-0.05Zr‡ (P896)	50.3	0.018	0.0015	0.021	0.048	0.28815	—	extrusion at 1400 K—16:1	12
NiAl-0.1Zr§ (P1187)	50.2	0.014	0.0018	0.049	0.094	0.28814	—	extrusion at 1400 K—16:1	9
NiAl-0.3Zr (P1423)	49.0	0.011	0.0006	0.079	0.28	0.28831	0.606	hipping at 1533 K—241 MPa for 5 h	50
NiAl-0.7Zr (P1424)	49.5	0.007	0.0006	0.079	0.74	0.28823	0.609	hipping at 1533 K—241 MPa for 5 h	41
NiAl (P541)	50.6	0.011	—	0.017	0.0	0.28836	—	extrusion at 1400 K—16:1	20 to 33[16,17]

†Standard deviations of ~1 μm for 0.05Zr and 0.1Zr and ~5 μm for 0.3Zr and 0.7Zr.
* ± 0.00004 nm.
** ± 0.002 nm.
‡Same lot of powder used in Refs. 16, 17, and 20.
§Also contains 0.005 at. pct Hf.

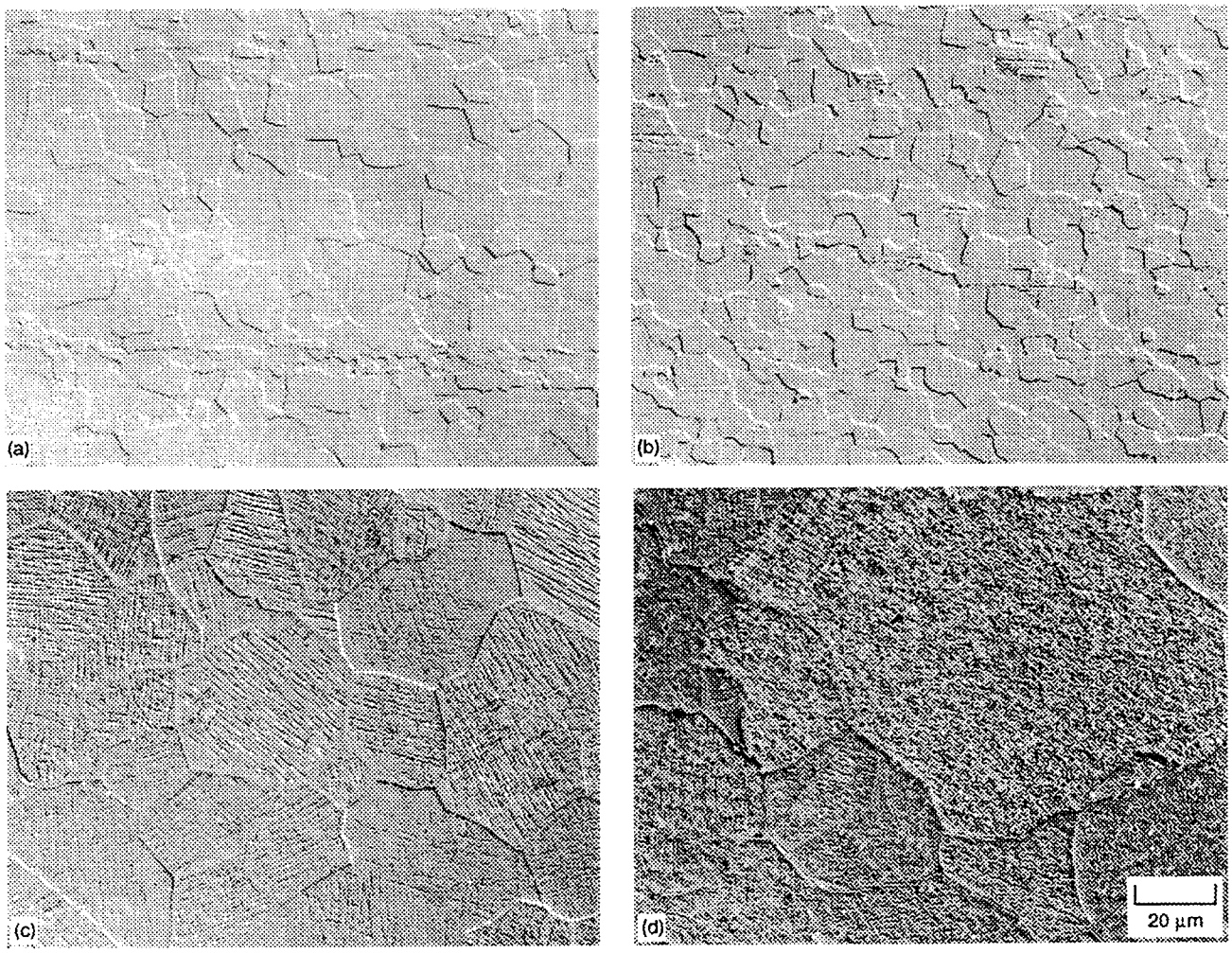

Fig. 1—As-received microstructure of NiAl containing various amounts of Zr: (*a*) 0.05Zr, (*b*) 0.1Zr, (*c*) 0.3Zr, and (*d*) 0.7Zr. The extrusion axis for samples (a) and (b) is horizontal.

In order to determine the ability of minor Zr alloying additions to provide strength at elevated temperatures, four heats of prealloyed NiAl containing from 0.05 to 0.7 at. pct Zr were obtained, consolidated, and compression tested at temperatures between 1000 and 1400 K at strain rates ranging from about 0.1 to 10^{-9} s^{-1}. In addition, faster strain rate ($>10^{-6}$ s^{-1}) testing of a binary NiAl between 900 and 1100 K was undertaken to provide a basis for comparison of strengths at lower temperatures. The results from the mechanical-property testing and its accompanying light optical metallographic studies are documented in this article.

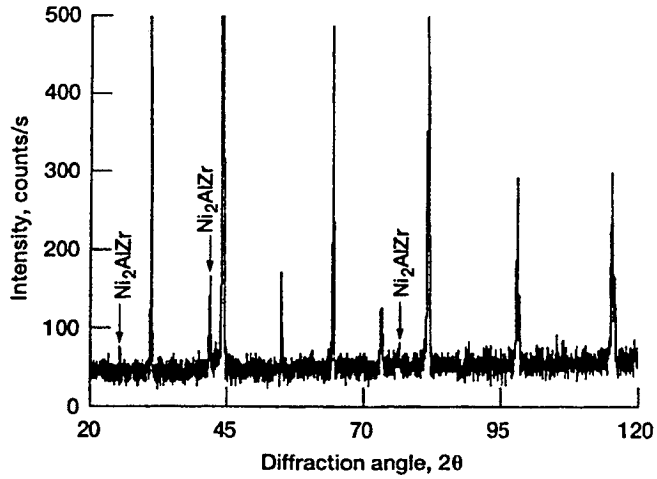

Fig. 2—X-ray diffraction intensity–diffraction angle scan from NiAl-0.7Zr. All peaks not specifically identified as Ni_2AlZr are from the NiAl matrix.

II. MATERIALS AND EXPERIMENTAL PROCEDURES

Four heats of prealloyed NiAl + Zr powder were purchased from Homogeneous Metals, Inc., Clayville, New York and sieved to a −100/+325 mesh size (Table I). Approximately 400 g of powder from each heat were vacuum sealed in 51-mm-diameter mild steel extrusion cans with a 6.3-mm wall thickness. While the 0.05 and 0.1Zr (all compositions are reported in at. pct) heats were successfully extruded at 1400 K with 16:1 reduction ratio, attempts to densify the 0.3 and 0.7Zr powders at 16:1, 12:1, or 8:1 reduction ratios were not successful. Hence, powders from the two higher Zr content alloys were vacuum sealed in thin-wall, 96-mm diameter by 150-mm long, stainless steel cans, which were subsequently consolidated by hot isostatic pressing ("hipping") at 1533 K and 241 MPa for 5 hours (Table I).

Typical microstructures of the four materials after densification are presented in Figure 1, which illustrate that all the alloys were fully consolidated after either extrusion (Figures 1(a) and (b)) or hipping (Figures 1(c) and (d)). Measurement of the grain sizes (Table I) revealed that the average dimension for the extruded alloys (0.05 and 0.1Zr) was about 10 μm, which was about a factor of four smaller than that for the hipped materials (0.3 and 0.7Zr). Under light optical microscopy conditions, no evidence of second phases could be seen in either of the low Zr-content alloys (Figures 1(a) and (b)); however, clear indications of precipitation were visible in the two higher Zr-containing materials (Figures 1(c) and (d)). X-ray diffraction examination of NiAl-0.7Zr (Figure 2, Table I) identified the precipitates as the Heusler-phase Ni_2AlZr in a NiAl matrix. Tentative identification of Ni_2AlZr precipitation was also made for NiAl-0.3Zr based on the appearance of one non-NiAl diffraction peak. The X-ray spectra for both NiAl-0.1Zr and NiAl-0.05Zr were indicative of single-phase, polycrystalline B2 crystal-structure materials.

The NiAl lattice parameters for all four alloys are consistent with the measured Al levels (Table I), as the lattice parameter values agree with those determined for near-stoichiometric, binary NiAl compositions.[4] In terms of impurities, the two higher Zr-content alloys contain much more oxygen than either NiAl-0.1Zr or NiAl-0.05Zr. On the other hand, NiAl-0.3Zr and NiAl-0.7Zr have slightly less carbon and nitrogen then the lower Zr-containing materials. Of these differences, it is probable that some of the oxygen in NiAl-0.3Zr and NiAl-0.7Zr is in the form of ZrO_2. Only NiAl-0.1Zr was found to contain any significant substitutional impurity; in this case, about 0.005 pct Hf was observed (Table I). As Hf is also a Heusler-phase former, the overall effect of this element is to bring the total amount of Ni_2AlX-forming elements to 0.1 pct.

Compression samples were fabricated by wire electrodischarge machining (EDM) about 5.5-mm diameter by ~55-mm long cylindrical bars with length parallel to the extrusion axis (0.05 and 0.1Zr) or long axis of the hot isostatic press can (0.3 and 0.7Zr). After the surface damage from EDM was removed by centerless grinding to a nominally 5-mm diameter, the 55-mm lengths were wire EDM cut into 10-mm-long sections. These were then made into true right cylinders by grinding the ends flat and parallel.

The compression specimens were subjected to both constant-velocity and constant-load creep testing in air at temperatures between 1000 and 1400 K. All specimens were tested in the as-consolidated condition. Constant velocity experiments were undertaken in a universal testing machine operating at speeds ranging from 2.1 mm/s to 2.1×10^{-4} mm/s, where the samples were loaded between two solid SiC rams. The autographically recorded load-time charts were converted to true stresses, strains, and strain rates *via* the offset method and the assumption of conservation of volume. The compressive creep response of the Zr-containing NiAl specimens was measured by a linear variable differential transducer (LVDT) which monitored the relative positions of the ceramic push bars applying a constant load. The contraction readings were stored in a data-acquisition system as a function of time. Following completion of each creep experiment, the results were normalized with respect to the final specimen length and converted into true stresses and strains by also assuming a constant volume.

As-received and selected post-tested specimens were metallurgically mounted as longitudinal sections, polished, and examined in a light optical microscope in the unetched and etched states. All materials were etched with a solution of 50 ml HF, 150 ml H_2O mixed with 100 g molybdic acid, and usually photographed under differential interference conditions (DIC) to improve grain-boundary definition for grain-size measurements.

III. RESULTS

A. *Mechanical Properties*

Examples of the true compressive stress-strain curves obtained from constant-velocity testing are presented in Figures 3 through 6. Behavior of all four materials is shown as a function of nominal strain rate for 1100 and 1300 K testing in Figures 3 and 4. These figures illustrate that the strength of the Zr-modified nickel aluminides decreases with decreasing strain rate at all test temperatures. Several general trends were noted. In particular, lower temperature and faster strain rates (Figure 3) led to continuous work hardening in all compositions. Also, higher temperature and slower strain rates (Figure 4) generally led to stress-strain

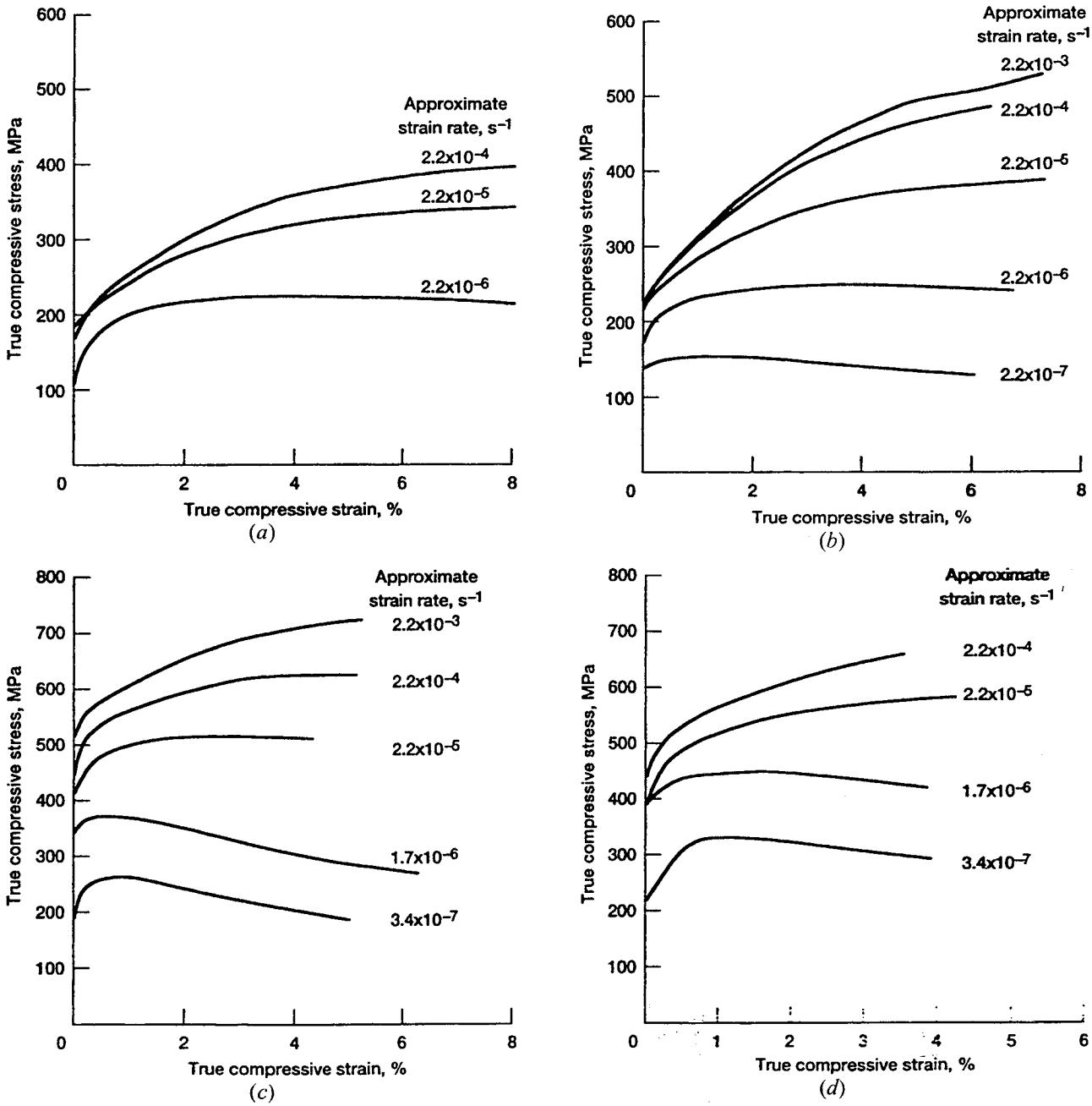

Fig. 3—True 1100 K compressive stress-strain curves as a function of strain rate for NiAl alloys containing (*a*) 0.05Zr, (*b*) 0.1Zr, (*c*) 0.3Zr, and (*d*) 0.7Zr.

diagrams with work hardening over the first 1 pct strain followed by continuous flow at a nominally constant stress. Occasionally, examples of work hardening to a maximum stress which was then succeeded by strain softening (Figures 3(c) and (d) and 4(c)) also were seen at all test temperatures.

The effect of Zr content on elevated-temperature strength is better demonstrated in Figures 5 and 6 for several temperature–strain rate combinations. Figure 5 illustrates the stress–strain behavior for the NiAl + Zr alloys at 1200 K but also is representative of behavior at lower temperatures. At these temperatures for both fast (Figure 5(a)) and slow (Figure 5(b)) strain rates, strength basically increases with increasing Zr level. This is no longer true for the Zr-containing alloys at and above 1300 K, where at each particular strain rate both the 0.3 and 0.7Zr alloys have approximately the same strengths (Figure 6). There still exists, however, a distinct difference in strength between simple solid-solution-hardened alloys and the two-phase compositions. This can be directly seen in Figure 6 and through comparison of the 1300 K stress-strain curves of the 0.05 to 0.1Zr alloys to those for 0.3 to 0.7Zr in Figure 5.

Typical compressive creep curves from the constant-load experiments are presented in Figure 7. All test conditions resulted in a small amount of primary strain followed by steady-state creep and in a few cases apparent tertiary creep. Nine of the ten creep tests were conducted under single-load conditions, while for the tenth sample (0.7Zr–1300 K, Figure 7(b)), the engineering stress was increased from 20 MPa to 31.2 MPa at ~420 ks. For all practical

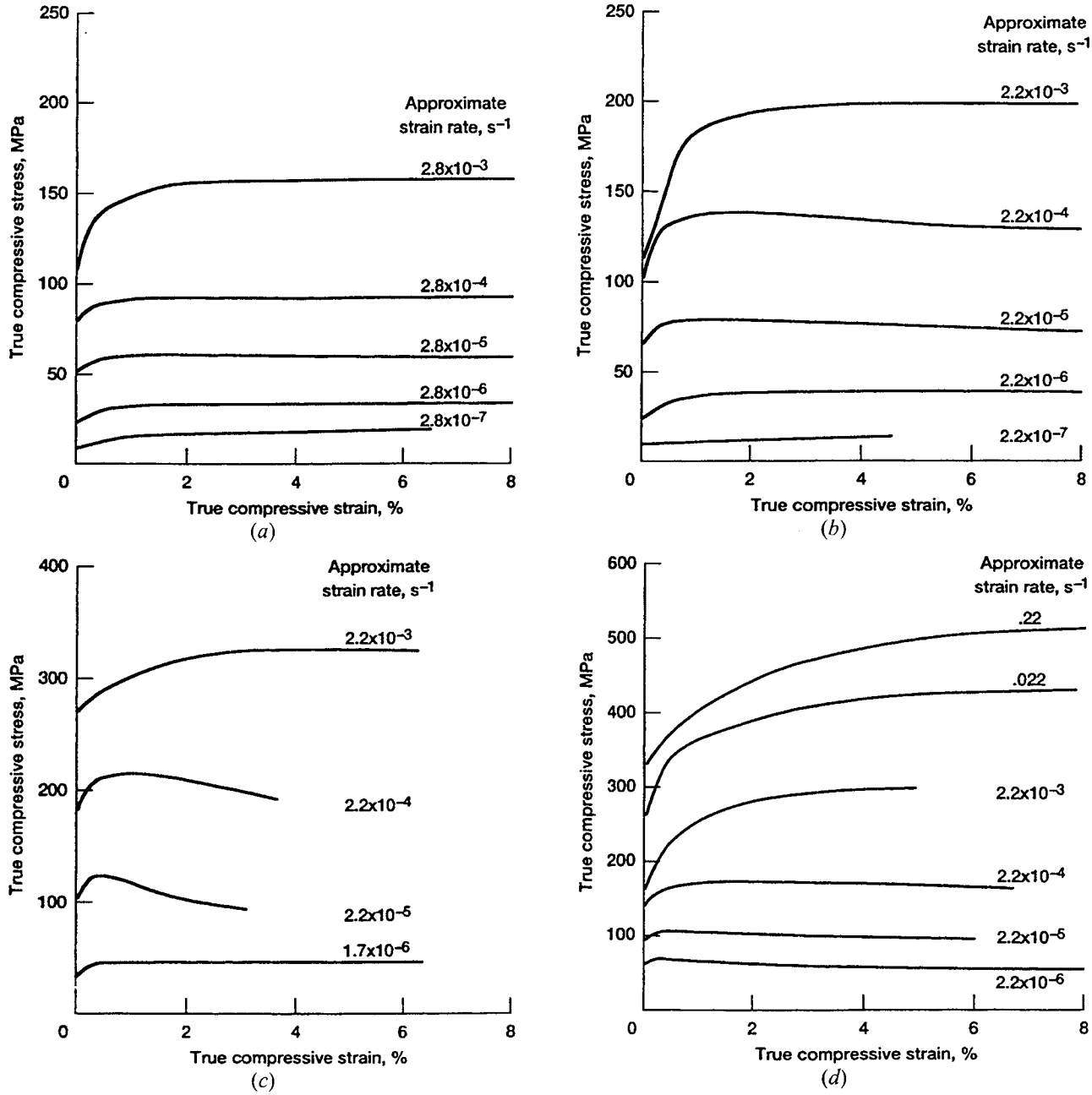

Fig. 4—True 1300 K compressive stress-strain curves as a function of strain rate for NiAl alloys containing (*a*) 0.05Zr, (*b*) 0.1Zr, (*c*) 0.3Zr, and (*d*) 0.7Zr.

purposes, this stress jump did not result in any transient creep at the higher stress level. It appeared that this specimen was in steady state prior to and immediately following the stress increase.

True compressive flow stress (σ)–strain rate ($\dot{\varepsilon}$)–temperature (T) behavior of the Zr-doped NiAl alloys is presented in Figure 8, where the flow stress was taken at 3 pct strain from the stress-strain diagrams (Figures 3 through 6) and from the steady-state regime of the creep curves (Figure 7). In addition to the present results, Figure 8(a) also contains some tensile test data (both constant-velocity and constant-load creep data) from Bowman and Noebe[23] for the same lot of NiAl-0.05Zr. Comparison of the tensile and compressive results for the 0.05Zr composition reveal little, if any, dependency on the test method or stress direction. Likewise, the constant-load compression creep results for 0.1Zr at 1200 K (Figure 8(b)) and the 1100 to 1400 K creep tests of 0.3Zr (Figure 8(c)) and 0.7Zr (Figure 8(d)) are consistent with the constant-velocity data.

Utilizing Figure 8(a) as an example, the σ-$\dot{\varepsilon}$-T properties appear to fall into three regimes: the fastest strain rate/lower temperature data follow a temperature-compensated exponential stress law (Eq. [1]); the slower strain rate/higher temperature data conform to a temperature-compensated power law (Eq. [2]); or, in some cases, the simpler constant-temperature version of Eq. [2].

$$\dot{\varepsilon} = A \cdot \exp(C\sigma) \cdot \exp(-Q/RT) \quad [1]$$

$$\dot{\varepsilon} = B \cdot \sigma^n \cdot \exp(-Q/RT) \quad [2]$$

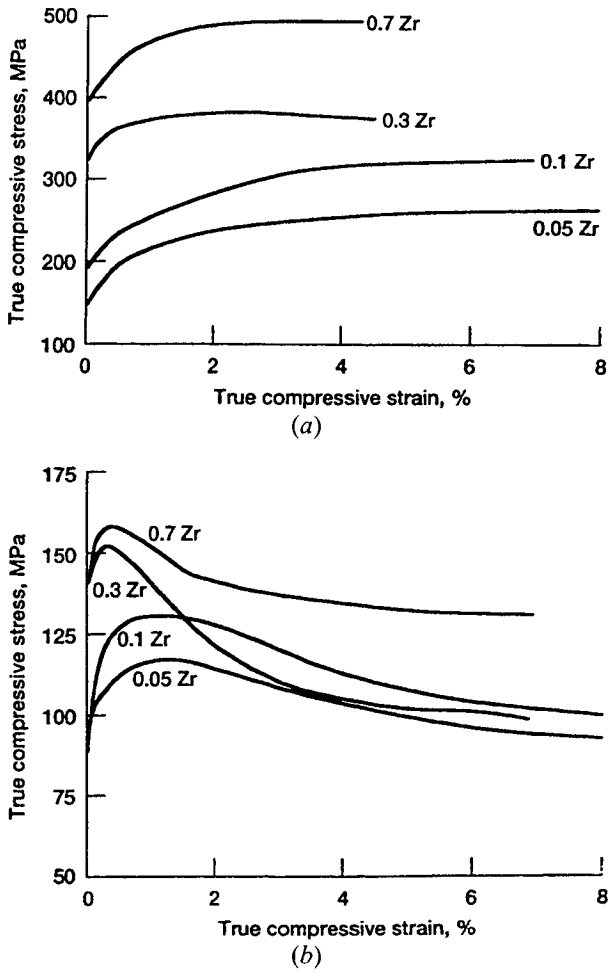

Fig. 5—True 1200 K compressive stress-strain curves for several NiAl alloys containing various amounts of Zr. Tested at a nominal strain rate of (*a*) 2.2×10^{-4} s^{-1} and (*b*) 2×10^{-6} s^{-1}.

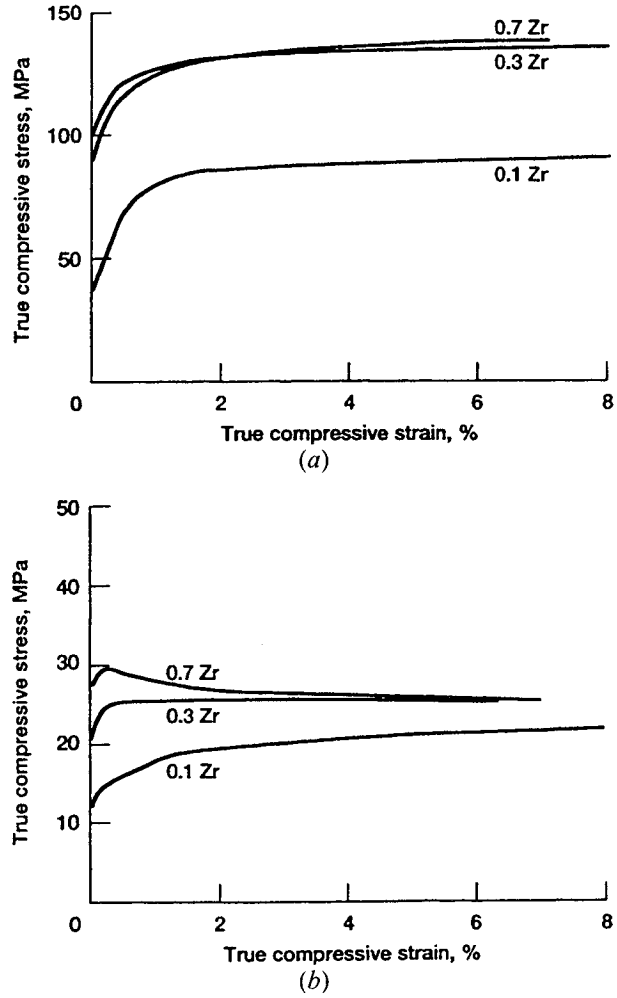

Fig. 6—True 1400 K compressive stress-strain curves for several NiAl alloys containing various amounts of Zr. Tested at a nominal strain rate of (*a*) 2.2×10^{-3} s^{-1} and (*b*) 2×10^{-6} s^{-1}.

In these equations, A and B are constants, C is the exponential stress constant, n is the stress exponent, Q is the activation energy, and R is the universal gas constant. Suitable groups of data were fitted to Eqs. [1] and [2] by linear regression techniques, and the resultant constants, stress exponents, activation energies, and appropriate statistical parameters, including the standard deviations for the stress constant (δ_C), stress exponent (δ_n), activation energy (δ_Q), and coefficient of determination (R_i^2), are listed in Table II. Additionally, the curves from the regression analyses are plotted in Figure 8, where the exponential stress fits (Eq. [1]) are shown as dashed lines and the power law fits (Eq. [2]) are represented by solid lines.

All four Zr-containing alloys possessed clearly defined temperature-stress regimes (Figure 8), where the temperature-compensated exponential law (Eq. [1]) was the appropriate descriptive equation. Application of the temperature-compensated power law (Eq. (2)), however, required some judgment. In particular, examination of the data for both solid-solution alloys (Figures 8(a) and (b)) strongly suggested that the stress exponent for the highest test temperature was different than that for the lower temperatures. Hence, the 1300 K results for NiAl-0.05Zr (Figure 8(a)) and the 1400 K data for NiAl-0.1Zr (Figure 8(b)) were fitted with the constant-temperature version of Eq. [2], while the lower-temperature data were simultaneously fitted as functions of temperature and stress. A similar change in deformation behavior was not observed for either the NiAl-0.3Zr (Figure 8(c)) or NiAl-0.7Zr (Figure 8(d)). Instead, Eq. [2] was applicable over all test temperatures for the two Heusler-containing alloys.

Both visually in Figure 8 and by the coefficient of determination in Table II, it can be seen that Eqs. [1] and [2] fit the experimental data reasonably well. The regimes of σ-$\dot{\varepsilon}$-T data currently described by the temperature-compensated exponential stress law in Figure 8 were also fitted to Eq. [2]; however, in each instance, the temperature-compensated power law analysis resulted in a poorer fit (Table II).

B. *Post-Test Microstructures*

Following compression testing, a number of samples were examined by light optical metallography techniques to assess changes in the microstructure. In the unetched condition, it was clear that the Zr-modified alloys were susceptible to internal oxidation with the degree of attack increasing with increasing Zr content. Overall, shorter term/lower temperature testing did not produce any damage, but longer term/higher temperature conditions led to

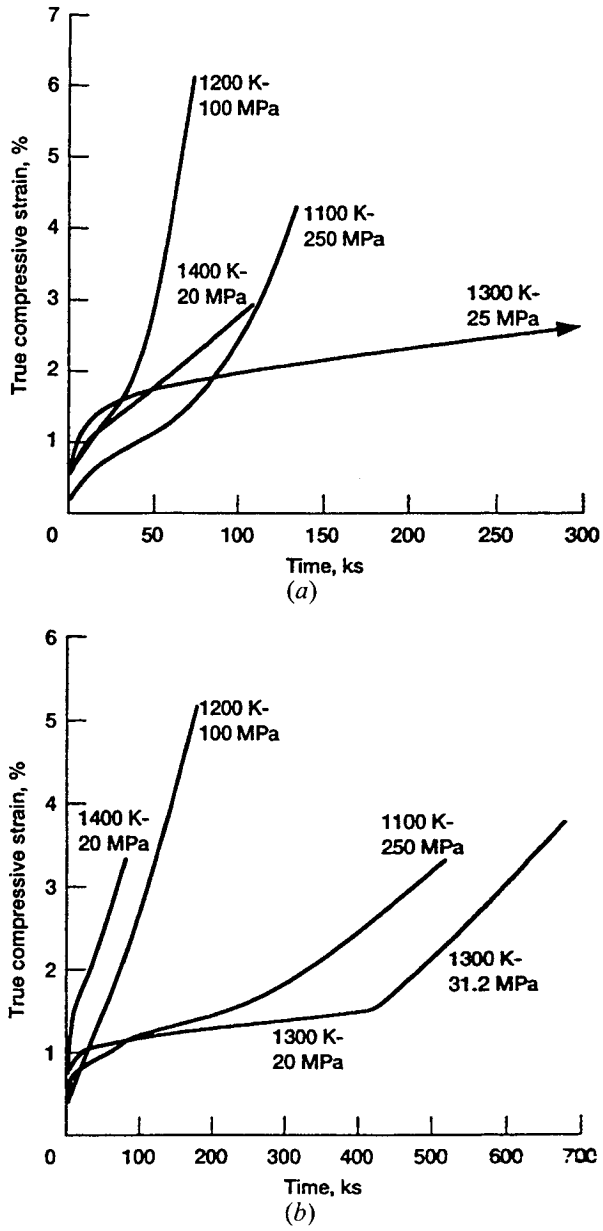

Fig. 7—True compressive creep curves for (*a*) 0.3Zr and (*b*) 0.7Zr NiAl-based alloys tested under a variety of conditions.

visible attack. Some examples of this behavior can be seen in Figure 9 for test specimens subjected to the highest temperature, longest term constant-velocity conditions. Minor intergranular oxidation was noted in 0.05Zr after very slow compression testing at 1300 K (Figure 9(a)) and 1200 K. Similar structures were also found in 0.1Zr after overnight testing at 1400 K (Figure 9(b)) and a 5-day experiment at 1300 K at $\sim 2 \times 10^{-7}$ s^{-1}. Little attack was seen in 0.1Zr following long-term 1200 K testing. Relatively severe internal oxidation, to a depth of about 100 μm, took place in both the 0.3Zr (Figure 9(c)) and 0.7Zr (Figure 9(d)) after being compressed for about 18 hours at $\sim 2 \times 10^{-6}$ s^{-1} and 1400 K. Reduction of the temperature to 1300 K did not diminish the degree of attack in overnight testing of 0.7Zr; however, only minor intergranular oxidation occurred in 0.3Zr compressed under similar conditions. Neither of these two-phase alloys exhibited any grain-boundary oxidation after 1200 K testing.

In general, little microstructural damage in terms of the formation of internal cracks or pores was seen in any tested samples; however, some short transverse and/or intergranular cracking was found near the specimen surfaces after fast strain rate/lower temperature testing of all alloys. Evaluation of the post-test grain sizes after a variety of test conditions (Table III) revealed little change from the as-received values (Table I). The only exceptions being the two solid-solution alloys after their severest (longest term, highest temperature) testing, where some grain growth appeared to take place.

IV. DISCUSSION

A. *Zr for Effective Strengthening*

The primary purpose of this work was to determine if polycrystalline Zr-modified NiAl possessed any significant elevated-temperature strength advantage over binary nickel aluminide. Comparison of the flow stress–strain rate behavior of the Zr-modified alloys to NiAl is presented in Figure 10. Because little $\dot{\varepsilon}$–σ data exists for binary NiAl at faster strain rates ($\dot{\varepsilon} \geq 10^{-5}$ s^{-1}) at and below 1100 K, constant-velocity testing of extruded Ni-50.6Al was undertaken between 900 and 1100 K. The results of this testing are reported in Appendix A and the appropriate data are utilized in Figure 10.

It is explicit in Figure 10 that Zr additions to NiAl promote significant strengthening at 1000 and 1100 K (Figures 10(a) and (b)); for example, the strength of NiAl-0.7Zr is eightfold that of binary NiAl. Furthermore, this advantage is maintained to very low strain rates at these two temperatures. At 1200 K (Figure 10(c)), however, the superior deformation resistance of NiAl alloyed with Zr begins to abate. The existing data demonstrate, for instance, that the strength advantage of NiAl-0.05Zr over NiAl at higher strain rates ($>10^{-5}$ s^{-1}) lessens as the deformation rates decrease. With another 100 K increase in temperature, the relative advantage of the Zr additions is further diminished, whereas at 1300 K (Figure 10(d)) NiAl-0.7Zr is only about three times stronger than NiAl in comparison to the factor of 8 increase at 1100 K (Figure 10(b)). Last, it can be seen at 1400 K (Figure 10(e)) that the strength advantage of the Zr-modified alloys is, at best, a factor of 2. For example, at a strain rate of 10^{-5} s^{-1}, the flow stress for NiAl-0.3/0.7Zr is ~40 MPa compared to ~20 MPa for binary NiAl. Also, it can be envisioned *via* extrapolation of the current 1400 K data that all the Zr-modified alloys and binary NiAl will have nearly equal strengths at a strain rate of about 10^{-8} s^{-1}.

In terms of the relationship between strength and Zr content, the results in Figure 10 clearly indicate that the two-phase alloys (0.3 and 0.7Zr) are stronger than the single-phase compositions (0.05 and 0.1Zr) and binary NiAl under all current test conditions. However, strength does not always scale in direct proportion with increasing Zr level. In general, increasing temperatures or decreasing strain rate diminish the importance of Zr. Certainly at 1100 K (Figure 10(b)), and presumably also at 1000 K (Figure 10(a)), strength at all strain rates increases with increasing

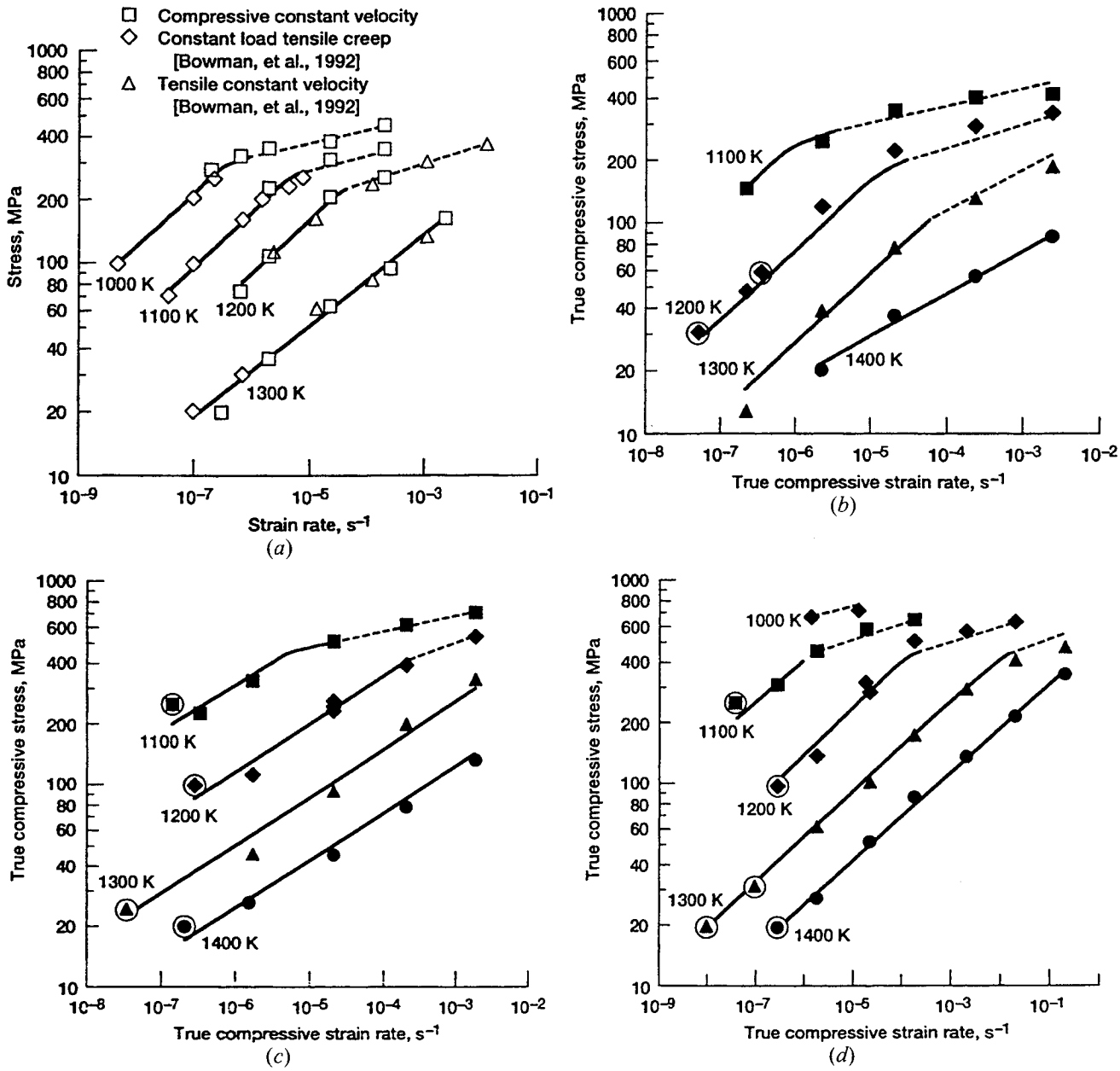

Fig. 8—True flow stress–strain rate behavior for NiAl alloys containing (*a*) 0.05Zr, (*b*) 0.1Zr, (*c*) 0.3Zr, and (*d*) 0.7Zr. Tensile results in (a) are from Ref. 23. Constant load compressive creep data points for (*b*) 0.1Zr, (*c*) 0.3Zr, and (*d*) 0.7Zr are encircled.

Zr content. But at 1200 K (Figure 10(c)), the two solid-solution alloys have similar strengths, while both two-phase alloys continue to order as their Zr content. At 1300 and 1400 K (Figures 10(d) and (e)), the 0.3 and 0.7Zr alloys demonstrate about the same resistance to deformation which is, in turn, somewhat better than the single-phase materials. Compared to the 1200 K results (Figure 10(c)), behavior of the 0.05 and 0.1Zr alloys at 1300 K (Figure 10(d)) is anomalous. In addition to the reemergence of the strength of 0.1Zr over 0.05Zr at fast strain rates, 1300 K testing also produced the situation where at $\sim 2 \times 10^{-7}$ s^{-1}, the flow stress of NiAl-0.1Zr was less than that for NiAl-0.05Zr or even NiAl. Because the grain size of NiAl-0.1Zr remained small (~ 10 μm) while that of NiAl-0.05Zr increased to 17 μm (Table III), it is likely that the low strength of NiAl-0.1Zr at 1300 K and $\sim 10^{-7}$ s^{-1} is due to an increasing contribution from grain-boundary deformation mechanisms similar to those observed in NiAl.[26,27]

The data in Figure 10, taken as a whole, demonstrate that Zr additions up to 0.7 pct in polycrystalline NiAl will not produce a significant improvement in creep behavior if applications at very high temperatures and slower strain rates are the objective. On the other hand, Zr can be quite advantageous for lower temperature deformation resistance. For example, at 1100 K (Figure 10(b)), even as little as 0.05Zr produces a large relative strengthening. However, to produce meaningful strength levels over a broader range of temperatures and strain rates, it appears that a distribution of Ni_2AlZr precipitates will be necessary. Thus, Zr concentrations greater than 0.1 pct will be required. However, the

Table II. Temperature-Compensated Exponential Law, Temperature-Compensated Power Law, and Power-Law Fits of the Flow Stress–Strain Rate Data for NiAl Alloys Containing Various Amounts of Zr

(a) Temperature-Compensated Exponential Law Analysis

Material	Number of Data Points	Temperature Range (K)	A (s^{-1})	C $(MPa)^{-1}$	Q (kJ/mol)	R_d^2	δ_c	δ_Q (kJ/mol)
NiAl-0.05Zr	12	1000 to 1200	9.97×10^{8}	0.0451	405	0.935	0.0052	35.9
NiAl-0.1Zr	9	1100 to 1300	5.17×10^{14}	0.0314	505	0.864	0.0056	75.8
NiAl-0.3Zr	5	1100 to 1200	7.26×10^{12}	0.0214	467	0.928	0.0045	102.3
NiAl-0.7Zr	8	1000 to 1200	1.97×10^{15}	0.0239	538	0.935	0.0055	57.2
NiAl	12	900 to 1100	1.40×10^{4}	0.187	317	0.917	0.020	36.1

(b) Temperature-Compensated Power-Law Analysis

Material	Number of Data Points	Temperature Range (K)	B (s^{-1})	n	Q (kJ/mol)	R_d^2	δ_n	δ_Q (kJ/mol)
NiAl-0.05Zr	17	1000 to 1200	9.03×10^{-2}	4.00	292	0.985	0.17	10.3
NiAl-0.1Zr	11	1100 to 1300	2.88×10^{5}	2.97	391	0.967	0.21	30.7
NiAl-0.3Zr	20	1100 to 1400	3.69×10^{5}	4.33	471	0.970	0.19	22.5
NiAl-0.7Zr	22	1100 to 1400	2.38×10^{8}	4.57	555	0.993	0.10	12.6
NiAl[20]	73	1100 to 1400	0.16	5.75	314	0.990	0.05	5.1

(c) Power-Law Analysis

Material	Number of Data Points	Temperature (K)	B (s^{-1})	n	R_d^2	δ_n
NiAl-0.05Zr	10	1300	7.76×10^{-14}	4.79	0.988	0.19
NiAl-0.1Zr	4	1400	1.05×10^{-12}	4.76	0.993	0.28
Ni-49.2Al[21]	3	1000	2.23×10^{-19}	6.85	0.999	0.18

current results (Figure 10) indicate that no real strength advantage exists for Zr contents above 0.3 pct, and the degree of damage from 1400 K oxidation suggests that an increase from 0.3 pct Zr (Figure 9(c)) to 0.7 pct Zr (Figure 9(d)) probably leads to a lowered environmental resistance due to internal oxidation. In view of the relatively minor oxidative attack in the 0.1 pct Zr alloy (Figure 9(b)) compared to the 0.3 pct Zr version (Figure 9(c)) after similar 1400 K testing as well as the near equivalence of elevated-temperature strength for the current two Heusler-strengthened materials, alloys with Zr contents between 0.1 and 0.3 pct should possess the optimum properties and would be worthy of further investigation.

Finally, it should be noted once again that both of the present two-phase alloys were tested in the as-hipped condition (1533 K–241 MPa–5 hours). If two-phase systems are the best choice for improving the mechanical strength at and below 1200 K, then heat-treatment studies that affect the precipitate size and distribution should be undertaken. Through analogy with γ'-strengthened Ni-base alloys, it is possible that the intermediate temperature strength of polycrystalline NiAl-Ni_2AlZr alloys can be significantly increased above current levels by appropriate heat treatments, perhaps combined with further alloying additions.

B. *Deformation Mechanisms in Zr-Modified NiAl*

The present study indicates that the Zr-modified materials are consistently stronger than binary NiAl and that the two-phase systems demonstrate real potential for intermediate temperature applications. Possible reasons for the increased strength of the Zr-modified alloys over binary NiAl can be found in the magnitudes of the deformation parameters listed in Table II. In particular, the activation energies from the temperature-compensated power law regime (Table II(b)) for the four Zr-modified alloys generally increase with increasing Zr content. This trend indicates that thermally activated deformation is becoming more difficult as the amount of Zr is increased. Such behavior could be partly due to a changing dislocation deformation mechanism as reflected in the stress exponents.

Creep in polycrystalline NiAl containing from 44 to 50.6 Al is dislocation climb controlled between 1100 and 1400 K, involving the formation of subgrains,[24] and this results in a stress exponent of about 5.8 (Table II(b)). Upon the addition of very small amounts of Zr to NiAl, dramatic decreases in the stress exponents are observed in both single-phase alloys at lower test temperatures: $n = 4$ for NiAl-0.05Zr between 1000 and 1200 K and $n = 3$ for NiAl-0.1Zr between 1100 and 1300 K (Table II(b)). In general, such stress exponents are indicative of a transition from climb-controlled creep to a viscous glide creep mechanism where the maintenance of an atmosphere of solute atoms around a dislocation inhibits its motion. At higher temperatures, however, both alloys demonstrate an apparent change to a higher stress exponent, where n is 4.8 for both NiAl-0.05Zr at 1300 K and NiAl-0.1Zr at 1400 K (Table II(c)). Thus, it appears that NiAl-Zr solid solutions undergo a class M to class A transition in creep mechanism (a change in stress exponent from about 5 to 3), as discussed by Langdon[28] for a number of metallic solid solutions.

Raj *et al.*[29] have studied deformation of the single-phase B2 alloy Ni-30Al-20Fe-0.05Zr between 1073 and 1300 K, and they observed a similar transition in stress exponent to that found in the 0.05 and 0.1 Zr-modified nickel alumin-

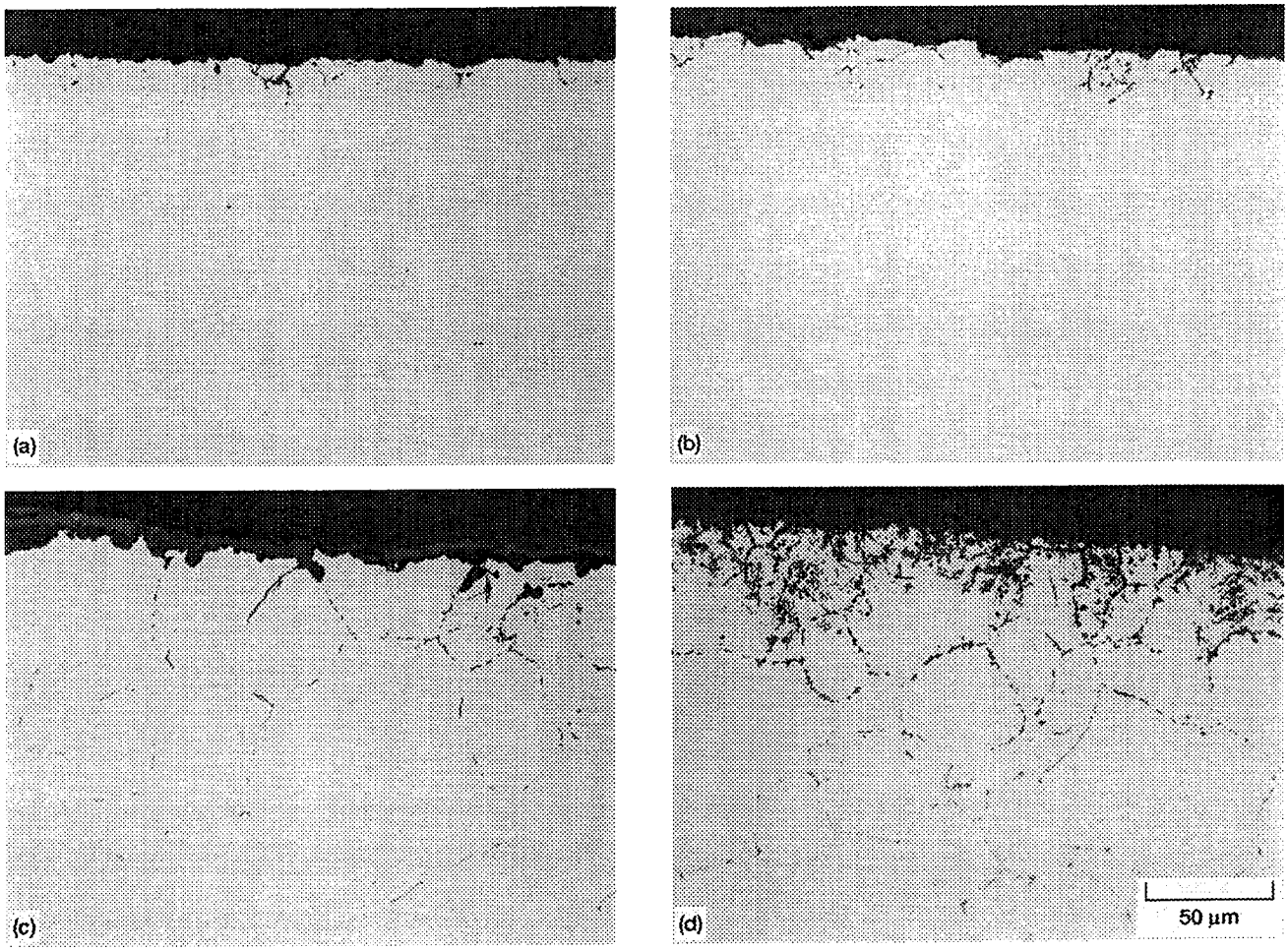

Fig. 9—Unetched near-surface microstructure of compression-tested Zr-modified NiAl. (*a*) 0.05Zr tested at 1300 K at 2.2×10^{-7} s^{-1} to 6.5 pct strain, (*b*) 0.1Zr tested at 1400 K at 2.2×10^{-6} s^{-1} to 8.5 pct strain, (*c*) 0.3Zr tested at 1400 K at 1.5×10^{-6} s^{-1} to 6.4 pct strain, and (*d*) 0.7Zr tested at 1400 K at 1.7×10^{-6} s^{-1} to 7.0 pct strain.

Table III. Post-Test Average Grain Dimensions for NiAl Alloys Containing Various Amounts of Zr

	Deformation Conditions													
Temperature, K	1000	1000	1100	1100	1100	1200	1200	1200	1300	1300	1300	1400	1400	1400
Strain Rate, s^{-1}	2×10^{-5}	2×10^{-7}	2×10^{-5}	2×10^{-6}	2×10^{-7}	2×10^{-5}	2×10^{-6}	2×10^{-7}	2×10^{-4}	2×10^{-6}	2×10^{-7}	2×10^{-3}	2×10^{-4}	2×10^{-6}
Material	Grain Size (μm)													
NiAl-0.05Zr	13	12	12	12	—	15	14	12	12*	—	17	not	tested	at 1400
NiAl-0.1Zr	not	tested	8	—	8	9	—	10	9	—	9	—	8	14
NiAl-0.3Zr	not	tested	50**	—	44	44	40	—	44	45	—	45	—	47
NiAl-0.7Zr	45	—	45	—	—	47	38	—	46	50	—	55	—	57

*Tested at 2×10^{-5} s^{-1}.
**Tested at 2×10^{-4} s^{-1}.

ides. Specifically, they reported two different power law stress exponent regimes (Table IV). Their 1073 K and faster 1200 K flow stress–strain rate results could be best described by an n of ~2.5, while the slower 1200 and 1300 K data exhibited a stress exponent of about 4.6. Raj *et al.* concluded that this transition from high stress exponent to a lower one with decreasing temperature or increasing stress was the result of a change in deformation mechanism from dislocation-climb to viscous glide-controlled creep. Furthermore, through comparison of their $n \approx 3$ data to various models for viscous glide creep, they concluded that glide-controlled creep in Ni-30Al-20Fe-0.05Zr could be described by the Cottrell–Jaswon model,[32] where the solid-solution strengthening was primarily due to Fe and not Zr.

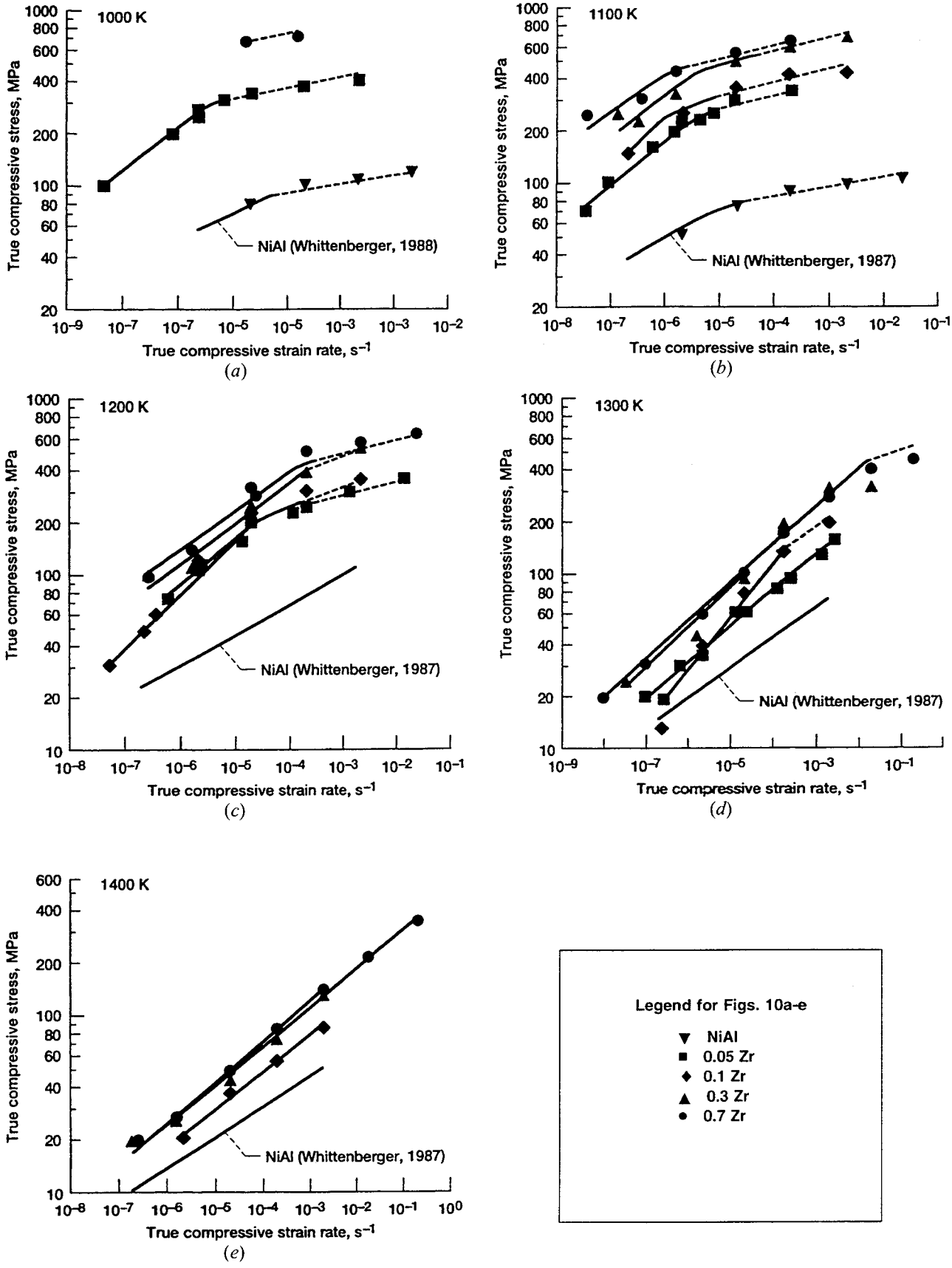

Fig. 10—Comparison of the flow stress–strain rate properties of the Zr-modified NiAl to binary NiAl as a function of temperature. (*a*) 1000 K, (*b*) 1100 K, (*c*) 1200 K, (*d*) 1300 K, and (*e*) 1400 K. Data for NiAl taken from the Appendix and Refs. 24 and 25.

Table IV. Temperature-Compensated–Power-Law Fits of Stress-Strain Rate Data for Single-Phase and Heusler-Strengthened NiAl Alloys

Composition (At. Pct)	Second Phase	Temperature Range (K)	Stress Exponent	Activation Energy (kJ/mol)	Reference
Ni-30Al-20Fe-0.05Zr	none	1073 to 1300	2.5 to 4.6	310	29
Ni-45Al-5Ti	none	1200 to 1300	3.05	385	30
Ni-40Al-10Ti	Ni_2AlTi	1200 to 1300	2.46	279	30
Ni-35Al-15Ti	Ni_2AlTi	1171 to 1419	3.53	275	12
Ni-47Al-0.8Hf	Ni_2AlHf	1200 to 1400	3	435	14
NiAl-1Hf (single-crystal)	Ni_2AlHf + G phase	1200 to 1400	4.13	379	6
Ni-49.5Hf-0.5Hf (single crystal)	Ni_2AlHf + G phase	—	—	454	31

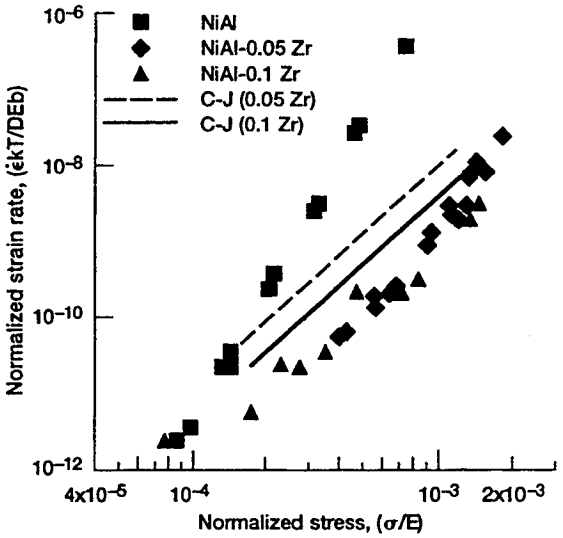

Fig. 11—(*a*) and (*b*) Comparison of the normalized creep rate and stress for NiAl and its alloys with the predicted behavior based on the Cottrell–Jaswon model of viscous glide controlled creep.

Following the reformulation of the Cottrell–Jaswon mechanism, as proposed by Raj *et al.*,[29] the normalized creep rate for viscous glide-controlled creep is given by

$$\dot{\varepsilon}\, kT/DEB = (18/e^2c) \cdot (kT/Eb^3)^2 \cdot (\sigma/E)^3 \qquad [3]$$

where k is Boltzmann's constant and c is the concentration of solute in mole fraction, and for NiAl alloys, the following apply:

D is the diffusion coefficient $\approx 10^{-4} \cdot \exp(-310{,}000/RT)$ in m^2/s;

E is the elastic modulus = $237{,}000 - 51T$ in MPa;[33]

b is the magnitude of the Burgers vector = 0.2876 nm; and

e is the solute-solvent size difference = 0.25 for Zr.

Normalized creep rates for NiAl as well as NiAl-0.05Zr and NiAl-0.1Zr are presented as a function of modulus normalized stress in Figure 11(a). For simplicity, the binary data were taken from 1100 to 1400 K testing of Ni-49.2Al,[25] and the Zr-modified results were restricted to those points in the $n = 3$ (NiAl-0.1Zr) or 4 (NiAl-0.05Zr) regime. These data point out the large differences in strength between binary NiAl and its Zr-modified alloys at high stresses and the apparent convergence of all the materials below $\sigma/E \approx 10^{-4}$. The Cottrell–Jaswon model predictions of the normalized creep rates (Eq. [3]) for NiAl-0.05Zr and NiAl-0.1Zr are represented by the dashed and solid lines, respectively, in Figure 11. These curves were calculated for 1200 K; estimates at higher or lower temperatures simply gave a series of very closely spaced, parallel lines bracketing the present two curves.

Although Figure 11(a) indicates that the actual strengths of NiAl-0.05/0.1Zr are greater than the predictions, these differences could simply be due to an error in the strain-rate normalization procedure. If, for example, the frequency factor in the diffusion equation was 2×10^{-5} m^2/s, instead of 10^{-4} m^2/s assumed by Raj *et al.*,[29] normalization brings the vast majority of the data for Zr-modified NiAl into coincidence (Figure 11(b)) with the Cottrell–Jaswon model.

Since a pre-exponential diffusion factor of 2×10^{-5} m^2/s is well within commonly accepted values for this constant, it appears that excellent agreement exists between theory and measurement. Therefore, viscous creep in NiAl-Zr solid solutions is probably controlled by Zr atmospheres around gliding dislocations.

Without detailed microstructural and heat-treatment studies, little can be said about the controlling deformation

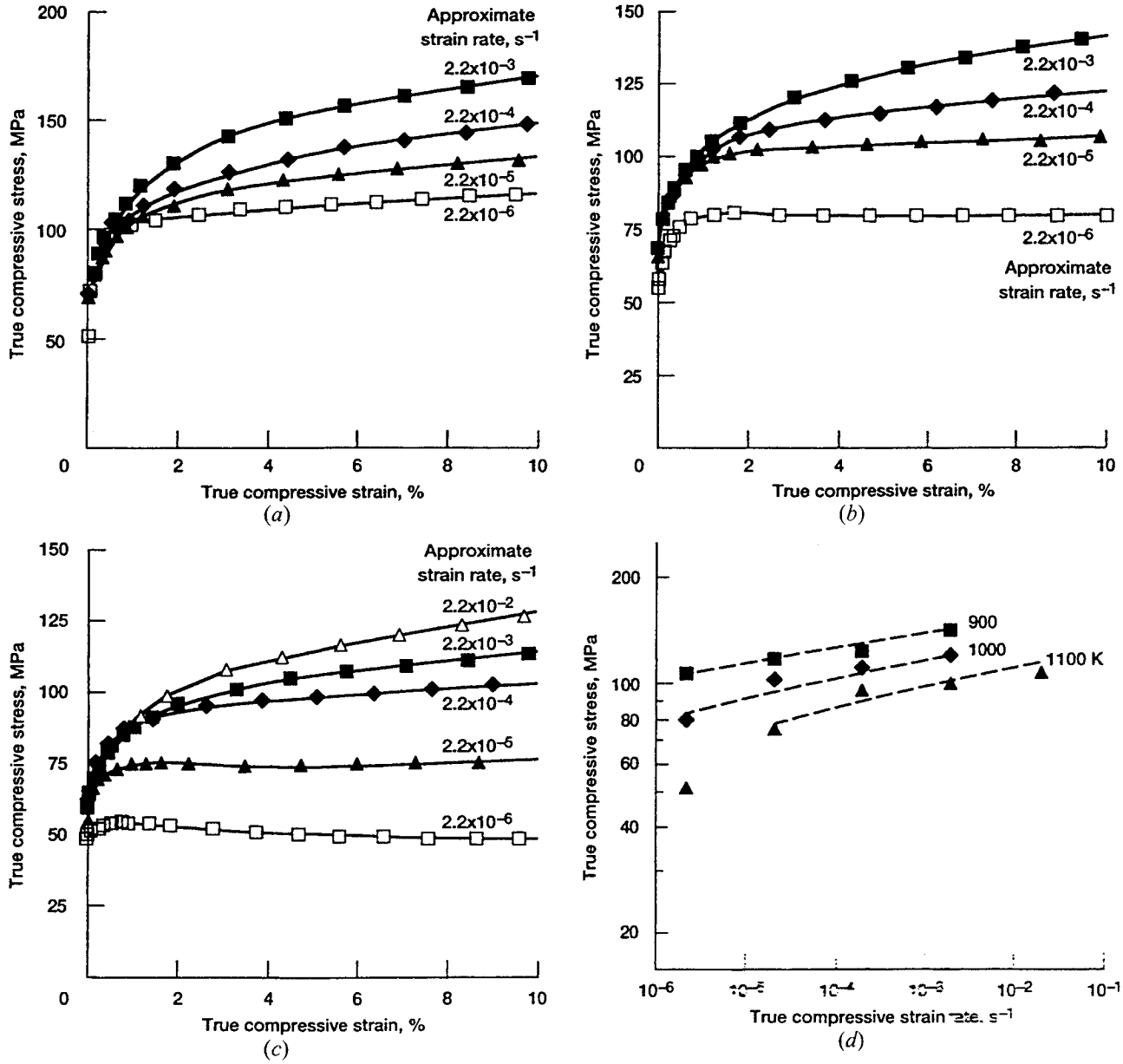

Fig. 12—True compressive stress–strain diagrams for Ni-50.6Al tested at (*a*) 900 K, (*b*) 1000 K, and (*c*) 1100 K as a function of nominal strain rate and (*d*) true compressive flow stress–strain rate–temperature behavior for Ni-50.6Al.

mechanisms in the two-phase Zr-modified alloys (NiAl-0.3Zr and NiAl-0.7Zr). The stress exponents and activation energies for these two materials are significantly different from those measured for other polycrystalline Heusler-strengthened nickel aluminides. For example, Ni_2AlTi-containing alloys have $n \sim 3$ and $Q \sim 300$ kJ/mol, while NiAl-Ni_2AlHf possesses a stress exponent of 3 and activation energy of 435 kJ/mol (Table IV). The present two-phase Zr-modified materials have both higher stress exponents ($n \approx 4.5$) and activation energies (($Q \approx 500$ kJ/mol) Table II(b)). In addition, both of the current Ni_2AlZr-strengthened alloys display similar mechanical properties, even though the volume fraction of Heusler precipitate in NiAl-0.7Zr is potentially three times that in NiAl-0.3Zr. Therefore, much work remains before a reasonable understanding of Zr-precipitation-strengthened NiAl can be suggested.

V. SUMMARY OF RESULTS

Elevated-temperature deformation has been examined between 1000 and 1400 K for a series of polycrystalline B2 crystal-structure nickel aluminides containing from 0.05 to 0.7 at. pct Zr. While any concentration of this third element is a potent strengthening agent under lower temperature and faster strain-rate conditions, the data for the single-phase alloys (Zr ≤ 0.1 at. pct) do not indicate much improvement over binary NiAl for higher temperature and slower strain rate applications.

The strengthening observed in the single-phase alloys are consistent with a mechanism by which Zr atmospheres control creep by a viscous glide process. Two-phase NiAl-Ni_2AlZr alloys, however, do display strength advantages over single-phase materials under all test conditions. Surprisingly, resistance to deformation was not significantly

affected by the amount of the second phase, with both NiAl-0.3Zr and NiAl-0.7Zr displaying similar mechanical properties. Oxidation resistance, on the other hand, was affected by Zr content, where the degree of microstructural damage was worst in the highest Zr-level alloy.

VI. CONCLUSIONS

Based on the strength properties and microstructural damage from oxidation of polycrystalline Zr-modified NiAl, it is concluded that optimum elevated-temperature behavior (high strength and adequate oxidation resistance) could be obtained in two-phase, Heusler-strengthened NiAl containing between 0.1 and 0.3 at. pct Zr.

APPENDIX
900 to 1100 K stress-strain–strain rate behavior of Ni-50.6Al

To extend the range of flow stress–strain rate–temperature data for binary NiAl, compression samples were cut from a bar of hot extruded Ni-50.6Al powder and tested under constant-velocity conditions between 900 and 1100 K in the same manner as described in Section II. The alloy composition, consolidation procedures, and grain size are noted in Table I. The same heat of material was also tested in References 16, 17, and 20.

True compressive stress–strain curves from the constant-velocity testing are presented as a function of temperature and nominal strain rate in Figures 12(a) through (c). These curves possess similar characteristics under all test conditions, where rapid work hardening occurs over the first ~2 pct strain and is followed by much slower strain hardening for the faster deformation/lower temperature conditions or by continued flow under an approximately constant stress. The flow stress–strain rate data, taken at 3 pct strain from Figures 12(a) through (c), are shown in Figure 12(d). With the exception of the slowest strain-rate result for 1100 K, the data could be adequately described by a temperature-compensated exponential law (Eq. [1]), and the appropriate parameters for this description are reported in Table II. The activation energy of 317 kJ/mol from this analysis is identical to the 314.2 kJ/mol activation energy reported for a temperature-compensated power law fit of 1100 to 1400 K data from NiAl containing from 44 to 50.6Al.[24]

REFERENCES

1. R. Darolia: *JOM*, 1991, vol. 43 (3), pp. 44-49.
2. C.T. Liu and K.S. Kumar: *JOM*, 1993, vol. 45 (5), pp. 38-44.
3. D.B. Miracle: *Acta Metall. Mater.*, 1993, vol. 41, pp. 649-84.
4. R.D. Noebe, R.R. Bowman, and N.V. Nathal: *Int. Mater. Rev.*, 1993, vol. 38, pp. 193-232.
5. R. Darolia: in *Structural Intermetallics*, R. Darolia, J.J. Lewandowski, C.T. Liu, P.L. Martin, D.B. Miracle, and M.V. Nathal, eds., TMS, Warrendale, PA, 1993, pp. 495-504.
6. I.E. Locci, R. Dickerson, R.R. Bowman, J.D. Whittenberger, M.V. Nathal, and R. Darolia: in *High-Temperature Ordered Intermetallic Alloys V*, I. Baker, R. Darolia, J.D. Whittenberger, and M.H. Yoo, eds., Materials Research Society, Pittsburgh, PA, 1993, vol. 288, pp. 685-90.
7. W.S. Walston, R.D. Field, J.R. Dobbs, D.F. Lahrman, and R. Darolia: in *Structural Intermetallics*, R. Darolia, J.J. Lewandowski, C.T. Liu, P.L. Martin, D.B. Miracle, and M.V. Nathal, eds., TMS, Warrendale, PA, 1993, pp. 523-32.
8. R.D. Noebe, R.R. Bowman, and M.V. Nathal: NASA TP-3398, 1994.
9. D.P. Mason, D.C. Van Aken, R.D. Noebe, I.E. Locci, and K.L. King: in *High Temperature Ordered Intermetallic Alloys IV*, L.A. Johnson, D.P. Pope, and J.O. Stiegler, eds., Materials Research Society, Pittsburgh, PA, 1991, vol. 213, pp. 1033-38.
10. E.P. George and C.T. Liu: *J. Mater. Res.*, 1990, vol. 5, pp. 754-62.
11. R.D. Noebe and A. Garg: *Scripta Metall. Mater.*, 1994, vol. 30, pp. 815-20.
12. R.S. Polvani, Wen-Shian Tzeng, and P.R. Strutt: *Metall. Trans. A*, 1976, vol. 7A, pp. 33-40.
13. K. Vedula, V. Pathare, I. Aslandis, and R.H. Titran: in *High-Temperature Ordered Intermetallic Alloys*, C.C. Koch, C.T. Liu, and N.S. Stoloff, eds., Materials Research Society, Pittsburgh, PA, 1985, vol. 39, pp. 411-21.
14. J.D. Whittenberger, M.V. Nathal, S.V. Raj, and V.M. Pathare: *Mater. Lett.*, 1991, vol. 11, pp. 267-73.
15. J.D. Whittenberger, L.J. Westfall, and M.V. Nathal: *Scripta Metall.*, 1989, vol. 23, pp. 2127-30.
16. S.V. Raj, R.D. Noebe, and R. Bowman: *Scripta Metall.*, 1989, vol. 23, pp. 2049-54.
17. R.R. Bowman, R.D. Noebe, S.V. Raj, and I.E. Locci: *Metall. Trans. A*, 1992, vol. 23A, pp. 1493-1508.
18. R.D. Noebe and M.K. Behbehani: *Scripta Metall. Mater.*, 1992, vol. 27, pp. 1795-1800.
19. M.V. Zeller, R.D. Noebe, and I.E. Locci: NASA CP-10051, 1990, pp. 21-1-21-17.
20. R.D. Noebe: NASA TM 106534, 1994.
21. R.D. Noebe, B.A. Lerch, and K.B.S. Rao: in *High Temperature Ordered Intermetallic Alloys VI. Part I*, J.A. Horton, I. Baker, S. Hanada, R.D. Noebe, and D.S. Schwartz, eds., Materials Research Society, Pittsburgh, PA, 1995, vol. 364, pp. 291-296.
22. C.A. Barrett: *Oxid. Met.*, 1988, vol. 30, pp. 361-90.
23. R.R. Bowman and R.D. Noebe: NASA–Lewis Research Center, Cleveland, OH, unpublished research, 1992.
24. J.D. Whittenberger: *J. Mater. Sci.*, 1987, vol. 22, pp. 394-402.
25. J.D. Whittenberger: *J. Mater. Sci.*, 1988, vol. 23, pp. 235-40.
26. S.V. Raj and S.F. Farmer: in *High-Temperature Ordered Intermetallic Alloys V*, I. Baker, R. Darolia, J. Daniel Whittenberger, and M.H. Yoo, eds., Materials Research Society, Pittsburgh, PA, 1993, vol. 288, pp. 647-52.
27. S.V. Raj and S.F. Farmer: *Metall. Mater. Trans. A*, 1995, vol. 26A, pp. 343-56.
28. T.G. Langdon: in *Strength of Metals and Alloys (ICSMA 6)*, R.C. Gifkins, ed., Pergamon Press, New York, NY, 1983, pp. 1105-20.
29. S.V. Raj, I.E. Locci, and R.D. Noebe: *Metall. Trans. A*, 1992, vol. 23A, pp. 1705-18.
30. J.D. Whittenberger, R.W. Viswanadham, S.K. Mannan, and K.S. Kumar: *J. Mater. Res.*, 1989, vol. 4, pp. 1164-71.
31. R.D. Field: General Electric Aircraft Engines, Cincinnati, OH, unpublished research, 1993.
32. A.H. Cottrell and M.A. Jaswon: *Proc. R. Soc.*, 1949, vol. A199, pp. 104-14.
33. M.R. Harmouche and A. Wolfenden: *J. Test. Eval.*, 1987, vol. 15, pp. 101-04.